Continuous Furfuryl Alcohol Production via Coupled Dehydrogenation-Hydrogenation over Supported Cu and Au Catalysts: A Consideration of Hydrogen Generation and Transfer

Continuous Furfuryl Alcohol Production *via* Coupled Dehydrogenation-Hydrogenation over Supported Cu and Au Catalysts: A Consideration of Hydrogen Generation and Transfer

Chiara Pischetola,[a] Laura Collado,[a] Roque Aguado-Molina,[a] Samuel Martín-Treceño,[a] Mark A. Keane[a] and Fernando Cárdenas-Lizana*[a]

Department of Chemical Engineering, School of Engineering and Physical Sciences, Heriot Watt University, Edinburgh EH14 4AS, Scotland

*corresponding author:

Tel.: +44(0)131 451 4115, *e*-mail: F.CardenasLizana@hw.ac.uk

Abstract

We have investigated the continuous (*P* = 1 atm, *T* = 453 K) coupled dehydrogenation/hydrogenation of 2-butanol/furfural for the simultaneous production of 2-butanone and furfuryl alcohol. A series of oxides (Al_2O_3, ZrO_2, SiO_2, TiO_2 and CeO_2) were used to support nano-scale Cu (mean size 2.2-2.8 nm from STEM) and tested in the dehydrogenation of 2-butanol. All the supported Cu catalysts promoted exclusive formation of the target 2-butanone. Hydrogen production was shown to correlate with the Lewis basicity of the oxide support and the highest rate was recorded for Cu/CeO_2. Conventional furfural hydrogenation (using an external supply of hydrogen) over ceria supported Au (mean size = 3.5 nm) was fully selective to furfuryl alcohol where less than 1% of the hydrogen supplied was utilised. Under the same reaction conditions, exclusive formation of 2-butanone and furfuryl alcohol and higher hydrogenation rate was achieved in the coupled process over physical mixtures of Au/CeO_2+Cu/Oxide (in N_2) where Cu → Au hydrogen transfer was favored by coke (from TGA). The combination Au/CeO_2+Cu/CeO_2 delivered a 70-fold higher hydrogenation rate, full H_2 utilisation and 215 times lower E-factor. Our results demonstrate *in situ* hydrogen generation *via* dehydrogenation as a sustainable alternative hydrogenation route to valuable products.

Key words: coupling, dehydrogenation-hydrogenation, 2-butanone, furfuryl alcohol, Au+Cu physical mixture

1. Introduction

Catalytic hydrogenation is a core process in the chemical industry that is typically conducted batch-wise in an excess of pressurised H_2 to maximise product yield [1]. Current hydrogen production involves high temperature reforming processes [2]. Issues of safe handling, sustainable synthesis (12 kg CO_2 generated per kg H_2) and (production and distribution) cost [2] are the drivers for the search of alternative hydrogen sources and/or hydrogen donors. Catalytic transfer hydrogenation typically employs an organic hydrogen carrier (*i.e.* sacrificial donor) in tandem with a homogeneous catalyst [3] where generation of stoichiometric quantities of organic waste requires multiple separation/purification steps to isolate the target product and facilitate catalyst reuse [3]. The potential of heterogeneous catalysts (*e.g.* Pd [4], Ru [5], Fe [6], Pt [7] and Cu [8]) has been flagged [9] but work to date has focused on batch liquid systems that suffer from high operating pressure (typically 20-45 bar) [10,11], formation of by-products [12] and separation requirements for catalyst reuse.

The feasibility of coupling endothermic and exothermic reactions over heterogeneous catalysts has been addressed in a recent review by Siddiki *et al.* [13]. We examine here an ambient pressure continuous coupling of (endothermic) non-oxidative dehydrogenation with (exothermic) hydrogenation to generate two valuable products without an external hydrogen supply. As shown in **Figure 1(a)**, dehydrogenation (Step **I**) releases hydrogen (with Product 1) that is transferred (Step **II**) and used in hydrogenation with the formation of Product 2 through Step **III**. This requires two different active sites for hydrogen production and utilisation. We have focused on the continuous dehydrogenation/hydrogenation of biomass-derived 2-butanol/furfural [14,15] to valuable 2-butanone (1.2 million tons world production per year [16]) and furfuryl alcohol (130,000 tons world production per year [17]) (**Figure**

1(b)), which can be readily separated by distillation due to the (90 K) difference in boiling points [18]. Prior work has established selective furfural→furfuryl alcohol hydrogenation over supported Au catalysts [19] while alcohol → carbonyl compound hydrogen transfer is possible through a Meerwein-Ponndorf-Verley (MPV) mechanism when the active sites for -OH and -C=O adsorption/activation are in close proximity [20]. Moreover, we have demonstrated viable coupling of (2-butanol→2-butanone) dehydrogenation with furfural hydrogenation over a physical mixture of Cu/SiO_2+Au/CeO_2 [21].

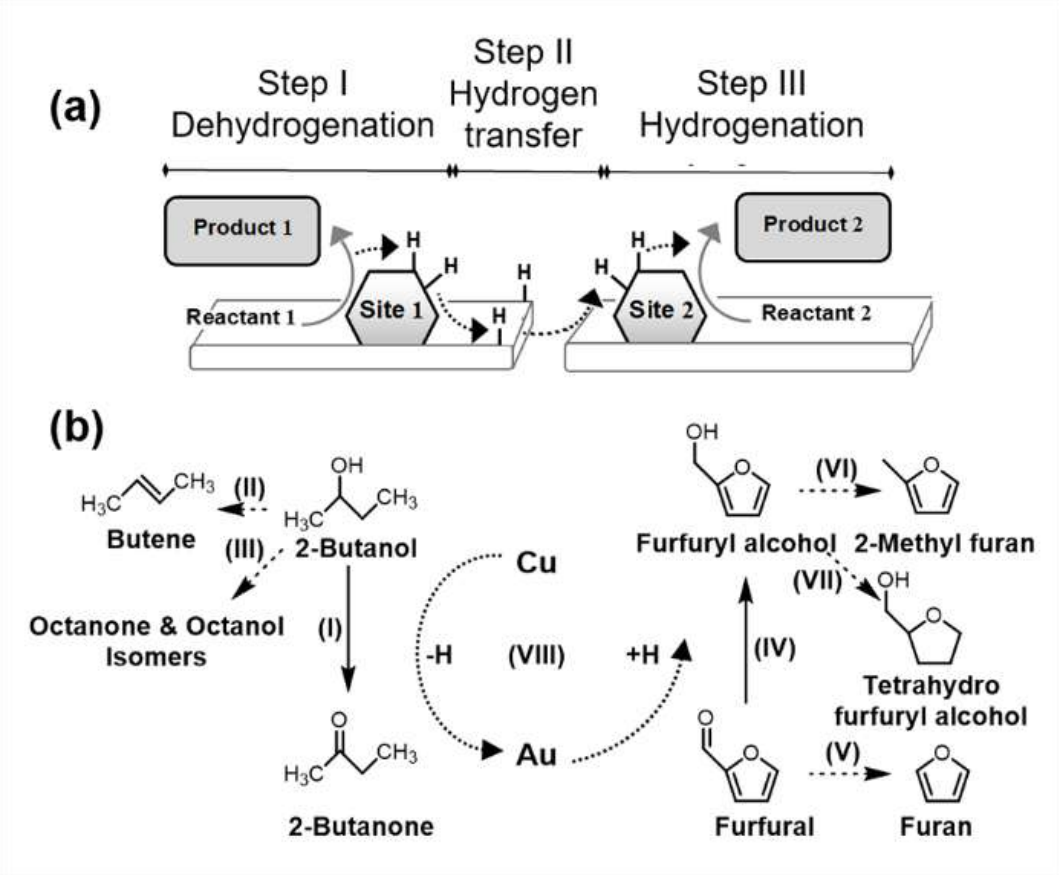

Figure 1. (a) Schematic for the proposed coupled process; **(b)** reaction scheme for 2-butanol dehydrogenation to the target **(I)** 2-butanone and undesired (**(II)** dehydration to butene and **(III)** dimerisation to octanone and/or octanol isomers) by-products, furfural hydrogenation to the target **(IV)** furfuryl alcohol and undesired (**(V)** decarbonylation to furan, **(VI)** hydrogenolysis to 2-methylfuran and **(VII)** ring reduction to tetrahydro-furfuryl alcohol) by-products and **(VIII)** coupled dehydrogenation-hydrogenation. *Note*: Solid arrows in **(b)** denote target reactions while dashed arrows indicate routes to undesired products and dotted arrows illustrate the coupled cycle, respectively.

Hydrogenation rate in the coupled system is governed by the supply of hydrogen which depends on the amount (i) generated in 2-butanol conversion and (ii) transferred across the surface of the carrier. Alcohol adsorption/activation occurs at the Cu-oxide interface with the hydrogen-end binding to support basic sites [22]. The studies that have quoted a catalytic response for alcohol (*e.g.* isopropyl [23] and benzyl alcohol [24]) dehydrogenation towards changes in catalyst basicity are scarce [23,24], although they point to higher activity with increased basicity. The Lewis basicity (capacity for electron donation) of the carrier can impact on the cleavage of the O-H bond, but we could find no reported correlation with hydrogen production. In addition, the redox nature of the oxide carrier can impact on the nature and mobility of hydrogen, as discussed in a recent paper by Wang *et al.* [25]. Up to date, most of the work has been conducted with pure H_2 over perfect/clean oxide surfaces [26] and under conditions that differ significantly from those in standard transfer hydrogenation reactions using homemade/commercial oxide carriers.

Herein, we evaluated the role of the support in determining hydrogen generation and transfer capacity with a view to maximising furfuryl alcohol production. We have examined a group of oxides (Al_2O_3, ZrO_2, SiO_2, TiO_2 and CeO_2) and address hydrogen utilisation efficiency by direct comparison with conventional hydrogenation using an external supply of hydrogen. The sustainability of the coupling process was quantified using the green metric environmental factor (E-factor, kg_{waste} $kg_{product}^{-1}$) [27].

2. Experimental

2.1 Materials

The supports employed in this study (Al_2O_3, ZrO_2, SiO_2, TiO_2 and CeO_2) were obtained from Sigma-Aldrich and used as received. All the gases used in this work

(O_2, H_2, N_2 and He) were of ultra high purity (>99.99%, BOC). Furfural (≥99%), furfuryl alcohol (≥99%), 2-methyl furan (99%), tetrahydrofurfuryl alcohol (99%), furan (≥99%), 2-butanol (≥99%), 2-butanone (≥99%), octanone (98%) and octanol (≥99%) were purchased from Sigma Aldrich and used without further purification.

2.2 Catalyst Preparation and Activation

Au/CeO_2 was prepared by deposition-precipitation using urea (99%, Riedel-de Haën) as basification agent. An aqueous solution of urea (100 fold excess) and $HAuCl_4$ (6×10^{-4} M, 300 cm^3; 99%, Sigma-Aldrich) was added to the support (5 g) and the suspension stirred and heated to 353 K under reflux (2 K min^{-1}). The pH progressively increased to reach 7 after 3-4 h as a result of thermal decomposition of urea. Copper on Al_2O_3, ZrO_2, SiO_2, TiO_2 and CeO_2 was prepared by an equivalent deposition-precipitation procedure using $Cu(NO_3)_2$ (3×10^{-3} M, 300 cm^3; 99%, Sigma-Aldrich) as metal precursor. The NaOH (2 M; ≥97%, Fisher Scientific) base was added to an aqueous solution of the metal precursor containing the support (5 g) until pH = 10, heated to 353 K and aged under vigorous stirring for 4 h to ensure homogeneous deposition of $Cu(OH)_2$ [28]. The solid was separated by filtration, washed with distilled water until pH = 7 and dried in 45 cm^3 min^{-1} He at 373-393 K overnight. The catalyst precursors were sieved (ATM fine test sieves) to mean particle diameter = 75 μm and activated at 2 K min^{-1} to 573 K in 60 cm^3 min^{-1} H_2. After activation, the catalysts were cooled to ambient temperature and passivated in 1% v/v O_2/He for off-line characterisation.

2.3 Catalyst Characterisation

The Au and Cu loading was determined by atomic absorption spectroscopy (AAS) using a Shimadzu AA-6650 spectrometer with an air-acetylene flame from the

diluted extract in aqua regia (25% v/v HNO_3/HCl). H_2-Temperature programmed reduction (H_2-TPR), H_2 chemisorption and total specific surface area (SSA) measurements were conducted on the commercial CHEM-BET 3000 (Quantachrome Instrument) unit with data acquisition/manipulation using the TPR Win^{TM} software (version 1.0). Samples were loaded into a U-shaped Pyrex glass cell (3.76 mm i.d.) and heated in 17 cm^3 min^{-1} (Brooks mass flow controlled) 5% v/v H_2/N_2 at 2 K min^{-1} to 573 K, swept with 65 cm^3 min^{-1} N_2 for 1.5 h, cooled to 453 K and subjected to H_2 chemisorption by pulse (10-20 µl) titration. In blank tests, there was no measurable H_2 uptake on the support alone. The SSA values were recorded with a (30 cm^3 min^{-1}) 50% v/v N_2/H_2 flow using the standard single-point BET method. Prior to analysis, the samples were outgassed at 423 K for 1 h in N_2. SSA and H_2 uptake values were reproducible to within ±5% and the values quoted in this paper are the mean. X-ray diffractograms (XRD) were recorded on a Bruker/Siemens D500 incident X-ray diffractometer using Cu Kα radiation, scanning at 0.02º per step over the range 10º ≤ 2θ ≤ 90º. The diffractograms were identified against the JCPDS-ICDD reference standards, *i.e.* CeO_2 (43-1002), Au (04-0784) and Cu (04-0836). Metal particle size and shape post-TPR was examined by scanning transmission electron microscopy (STEM) on a JEOL ARM 200CF operated at an accelerating voltage of 200 kV. The scanned images were collected using either Gatan 806 High Angle Annular Dark Field, Gatan 805 Annular Dark Field/Bright Field or JEOL ADF1 detectors under the control of a Gatan DigiScan II, employing Gatan DigitalMicrograph software (version 2.31) for data acquisition/manipulation. Samples were prepared for analysis by dry deposition on a holey carbon/Ni grid (300 Mesh). The surface area weighted mean metal size (*d*) was based on a count of up to 800 particles:

$$d = \frac{\sum_i n_i \cdot d_i^3}{\sum_i n_i \cdot d_i^2} \quad \textbf{(1)}$$

where n_i is the number of particles of diameter d_i. Thermogravimetric analysis (TGA) before and after reaction was employed to determine the presence and type (*e.g.* light hydrocarbons (soft coke) at 473 ≤ T < 673 K, bulky hydrocarbons (hard coke) at 673 ≤ T < 873 K and carbon layers at T ≥ 873 K, [29,30]) of carbonaceous materials [29,30] deposited on the catalyst surface as a result of reactant/product decomposition [31] using a LINSEIS STA PT 1600 instrument equipped with a Type S 240 furnace (RT-1773 K). Samples (13×10^{-3} – 23×10^{-3} g) were placed in an alumina crucible (*i.d.* = 7 mm, volume 0.3 cm^3) and heated in 100 cm^3 min^{-1} N_2 (Platon NGX), at 10 K min^{-1} to 973 K.

2.4 Catalytic System

Reactions (stand-alone hydrogenation of furfural (in H_2), independent dehydrogenation of 2-butanol (in N_2) and coupled dehydrogenation/hydrogenation of 2-butanol/furfural (in N_2)) were carried out at atmospheric pressure and 453 K, *in situ* after catalyst activation in a continuous flow fixed-bed tubular reactor (*i.d.* = 15 mm). Reaction conditions were selected to ensure negligible internal/external mass and heat transfer limitations. A layer of borosilicate glass beads served as preheating zone where the organic reactant(s) was(were) vaporised and reached reaction temperature before contacting the catalyst bed. Isothermal conditions (±1 K) were maintained by diluting the catalyst with ground glass (75 μm). Catalytic performance in a two bed arrangement (Cu/CeO_2 on the top bed and Au/CeO_2 in the bed below) was examined where each bed was separated by layer (15 mm) of glass wool; catalyst activation followed the procedure described above. Reaction temperature

was continuously monitored by a thermocouple inserted in a thermowell within the catalyst bed. The reactant(s) was(were) delivered to the reactor at a fixed flow (2×10^{-2} cm^3 min^{-1}) *via* a glass/teflon air-tight syringe and teflon line using a microprocessor controlled infusion pump (Model 100 kd Scientific). Dehydrogenation was conducted in a co-current flow of N_2 (20 cm^3 min^{-1}) with 2-butanol at *GHSV* (*i.e.* ratio of inlet gas flow rate (organic(s)+N_2 or H_2) to catalyst bed volume) = 3×10^3 h^{-1} and molar Cu (or Au, *n*) to reactant feed rate (*n*/*F*) = $2 \times 10^{-4} – 4 \times 10^{-4}$ h. Stand-alone hydrogenation was carried out in a co-current flow of H_2 (20 cm^3 min^{-1}) with furfural maintained at *GHSV* = 3×10^3 h^{-1} with *n*/*F* = 1×10^{-3} h, where the H_2 content was 90 times in excess to the stoichiometric requirement for furfuryl alcohol production. The coupled reaction was conducted in N_2 (20 cm^3 min^{-1}) at *GHSV* = 3×10^3 h^{-1}, *n*/*F* = $8 \times 10^{-5} – 3 \times 10^{-4}$ h, with Cu:Au molar ratio in the range of 12-48. In a series of blank tests, passage of each reactant in a stream of H_2 or N_2 through the empty reactor or over the (Al_2O_3, ZrO_2, SiO_2, TiO_2 and CeO_2) support alone or in a H_2 flow (stoichiometric H_2/Furfural molar ratio = 1) over Au/CeO_2 did not result in any detectable conversion. The reactor effluent was analysed by capillary GC (Perkin-Elmer Auto System XL gas chromatograph equipped with a programmed split/splitless injector and a flame ionisation detector, employing a DB-1 (50 m × 0.33 mm i.d., 0.20 μm film thickness) capillary column (J&W Scientific)). Data acquisition and manipulation were performed using the TurboChrom Workstation (version 6.3.2) chromatography data system. Reactant and product molar fractions (x_i) were obtained using detailed calibration plots (not shown). Reactant (i) conversion (X_i) is defined by:

$$X_i\textbf{(\%)} = \frac{[\text{reactant}]_{i,in} - [\text{reactant}]_{i,out}}{[\text{reactant}]_{i,in}} \times 100 \qquad \textbf{(2)}$$

and selectivity (*S*) to product (j) is given by:

$$S_j\textbf{(\%)} = \frac{[\text{product}]_{j,out}}{[\text{reactant}]_{i,in} - [\text{reactant}]_{i,out}} \times 100 \quad \textbf{(3)}$$

where the subscripts “in” and “out” refer to the inlet and outlet gas streams, respectively. Catalytic activity is also quantified in terms of (i) initial rate ($R_{reaction,process}$), obtained from time on-stream measurements as described elsewhere [32], according to:

$$R_{reaction,process} = \frac{F \cdot X_i}{n} \quad \textbf{(4)}$$

where the subscripts “reaction” and “process” refer to the dehydrogenation (D) or hydrogenation (H) reactions in the coupling and/or stand-alone processes and (ii) turnover frequency (*TOF*, h^{-1}; rate per active site) calculated based on metal dispersion from microscopy analysis as described elsewhere [33]. Hydrogen utilisation efficiency in the stand-alone hydrogenation *vs.* coupled process was assessed by:

$$H_2 \text{ utilization efficiency} = \frac{H_2 \text{ supplied}}{H_2 \text{ consumed}} \quad \textbf{(5)}$$

where H_2 supplied is the amount provided ((i) from an external gas cylinder supply or (ii) *via* alcohol dehydrogenation) while H_2 consumed represents the molar hydrogen utilised in the conversion of furfural. Repeated reactions using different samples from the same batch of catalyst delivered raw data reproducibility and mass balance within ±7%.The E-factor was determined according to the method described by Sheldon [27], as the ratio of waste produced (*i.e.* mass of unreacted furfural+2-

butanol+H_2+N_2 in the outlet gas stream) to product synthesised (*i.e.* furfuryl alcohol+2-butanone).

3. Results and Discussion

3.1 Conventional Stand-alone Furfural Hydrogenation

The physico-chemical properties of the Au/CeO_2 catalyst are presented in **Table 1**. Total specific surface area (SSA) was lower than the ceria support (49 m^2 g^{-1}), suggesting pore blockage by the metal component [34].

Table 1. Physico-chemical characteristics of the Au/CeO_2 catalyst.

		Au/CeO_2
Metal loading [% wt.]		1
SSA [m^2 g^{-1}]		40
H_2-TPR	***T_{max}* [K]**	420
	H_2 consumption [µmol g^{-1}]	299[a]/69[b]
***d* [nm]**		3.5 ± 0.9
H_2 chemisorption [µmol g_{metal}^{-1}][c]		65

[a]from TPR measurement; [b]theoretical for $Au^{3+} \rightarrow Au^0$; [c]Au; [c]H_2 titration at 453 K.

The H_2 temperature programmed reduction (H_2-TPR) profile for Au/CeO_2 (**Figure 2(I)**) presents a maximum at 420 K with a 4-fold greater H_2 consumption relative to the amount required for the $Au^{3+} \rightarrow Au^0$ reduction (**Table 1**), indicative of partial support reduction at the Au-CeO_2 interface [35].

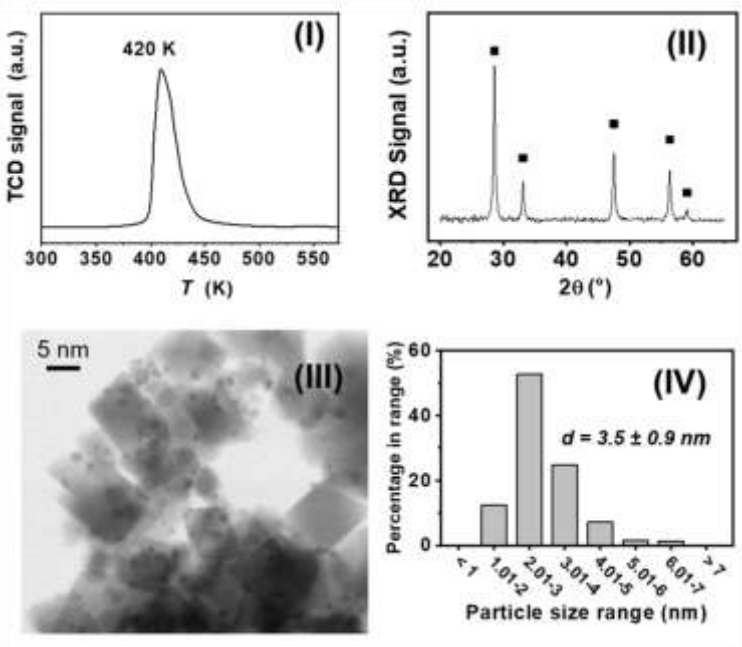

Figure 2: Au/CeO_2; **(I)** H_2-TPR profile, **(II)** XRD pattern, **(III)** representative STEM image with **(IV)** associated Au particle size distribution. *Note*: XRD peak assignments in **(II)** based on JCPDS-ICDD reference data: (■) CeO_2 (43-1002).

The powder X-ray diffraction (XRD) pattern of Au/CeO_2 (**Figure 2(II)**) matched that of CeO_2 with a cubic fluorite structure (JCPDS-ICDD reference 43-1002). There were no detectable diffraction peaks for gold, suggesting metal nanoparticles <5 nm [36]. The representative scanning transmission electron microscopy (STEM) image (**Figure 2(III)**) confirms the formation of nano-scale Au particles (**Figure 2(IV)**) with a mean size of 3.5 nm. Small (≤5 nm) gold nanoparticles with a high concentration of (low-coordination) Au edge and corner positions [37,38], active sites for hydrogen adsorption/activation [39], are essential for significant catalytic activity in hydrogenations [37].

In standard furfural hydrogenation using an external supply of H_2, Au/CeO_2 promoted exclusive furfural → furfuryl alcohol transformation. In contrast, decarbonylation (to furan (path **V**) in **Figure 1(b)**), hydrogenolysis (to 2-methylfuran (path **VI**)) and/or ring reduction (to tetrahydro furfuryl alcohol (path **VII**)) have been

reported for gas phase reaction over (Ta_2O_5, SiO_2, Al_2O_3, TiO_2) supported Pt, Ni and Pd catalysts [40]. The Au/CeO_2 catalyst exhibited a decline in conversion to reach a pseudo-steady state after *ca.* 2 h on-stream (see **Figure S1** in Supporting Information). The extracted specific furfuryl alcohol production rate (*TOF* = 171 h^{-1}) was significantly greater than that recorded under similar reaction conditions (453 K) over (SiO_2) supported Pt (133 h^{-1} [41]) and Ni (<1 h^{-1} [42]) catalysts. High selectivity to the target alcohol is a crucial requirement but H_2 utilisation must also be addressed in terms of overall process sustainability [43]. Less than 1% of the H_2 supplied was used in hydrogenation over Au/CeO_2 (*i.e.* 3 × 10^{-5} mol h^{-1} consumed *vs.* 32 × 10^{-3} mol h^{-1} supplied) with a high associated E-factor = 430, indicative of serious inefficiency [27]. Hydrogen dissociation is rate-determining in aldehyde hydrogenation over Au [44] and the low hydrogen utilisation can be attributed to a limited capacity of Au to chemisorb and activate hydrogen [45]. This is consistent with the significantly lower H_2 uptake for Au/CeO_2 (65 μmol g_{metal}^{-1}; **Table 1**) relative to values reported for supported Pd and Pt catalysts with similar metal loading (1460-1870 μmol g_{metal}^{-1}) [46,47].

Atomic hydrogen is generated stepwise during alcohol dehydrogenation over zero valent transition metal (*e.g.* Ni, Pt, Cu) catalysts [48-50]. This active form generated *in situ* can migrate from the metal nanoparticle to the support, along the oxide surface [51] and across solid/solid grain boundaries [52], to participate in hydrogenation [53] (Step **II** in **Figure 1(a)**). This supply of active hydrogen in the coupling dehydrogenation-hydrogenation circumvents the limitations associated with H_2 activation by Au while retaining the inherent reaction selectivity. An essential requirement for effective coupling is that dehydrogenation proceeds at an equivalent or greater rate than hydrogenation to ensure sufficient hydrogen supply. There was

no detectable activity in stand-alone dehydrogenation (2-butanol in N_2) using Au/CeO_2 and a second metal is required to promote hydrogen generation from 2-butanol transformation. Copper supported on oxides [54-56] and carbon [57] is effective in gas phase (423-573 K) dehydrogenation (of cyclohexanol [54,55], *n*-pentanol [56] and ethanol [57]) and was accordingly chosen as our test catalyst.

3.2 Hydrogen Generation from 2-Butanol Dehydrogenation

A range of oxide carriers were chosen to evaluate the effect of the support on hydrogen production for a similar Cu loading (2-4% wt., **Table 2**).

Table 2. Physico-chemical characteristics of the oxide supported Cu catalysts.

		Cu/Al_2O_3	Cu/ZrO_2	Cu/SiO_2	Cu/TiO_2	Cu/CeO_2
Metal loading [% wt.]		2.5	3.3	2.7	1.9	3.5
SSA [m^2 g^{-1}]		143	52	201	47	38
H_2-TPR	**T_{max} [K]**	497	481	527	423	453
	H_2 consumption [μmol g^{-1}]	340[a]/393[b]	526[a]/519[b]	447[a]/425[b]	336[a]/299[b]	701[a]/551[b]

[a]from TPR measurement; [b]theoretical for $Cu^{2+} \rightarrow Cu^0$.

The total surface area, which ranged from 38 m^2 g^{-1} (Cu/CeO_2) to 201 m^2 g^{-1} (Cu/SiO_2), is in agreement with values recorded elsewhere [58,59]. The H_2-TPR profiles are presented in **Figure 3** where the H_2 consumed (**Table 2**) was close to the requirement for Cu^{2+} reduction to Cu^0. We observed a shift in the temperature of maximum H_2 consumption (T_{max}) during H_2-TPR from 481-527 K for Cu supported on non-reducible $ZrO_2/Al_2O_3/SiO_2$ to 423-453 K for Cu on reducible TiO_2/CeO_2. A similar trend of lower temperature reduction of Cu on TiO_2 *vs.* SiO_2/Al_2O_3 [60] and CeO_2 *vs.* Al_2O_3 [61] has been reported and attributed to strong metal-support interactions [62], resulting in a more facile reduction of the (Cu^{2+}) precursor on reducible supports [63].

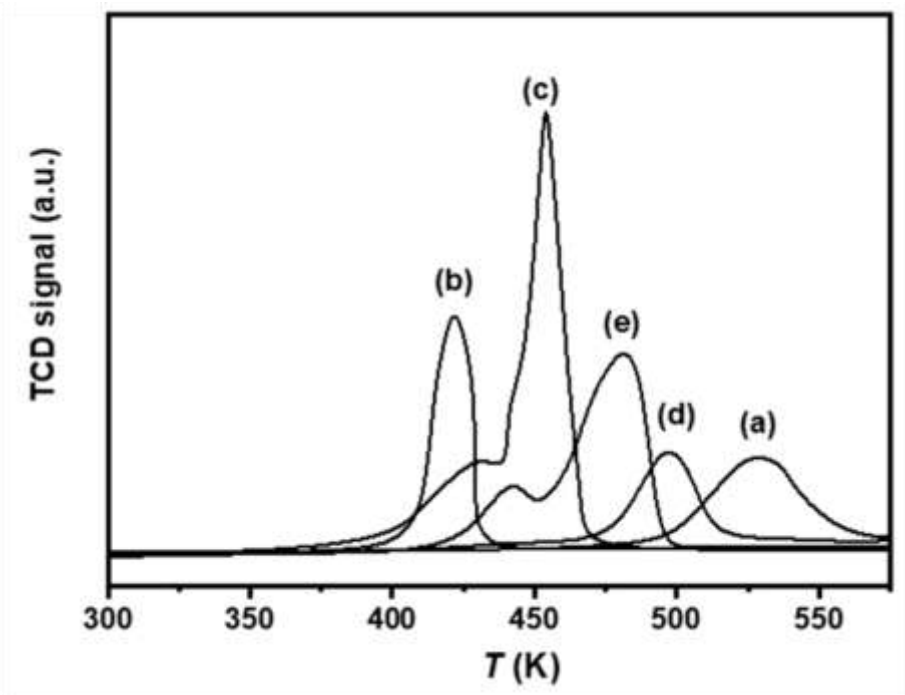

Figure 3. H_2-TPR profiles for **(a)** SiO_2, **(b)** TiO_2, **(c)** CeO_2, **(d)** Al_2O_3 and **(e)** ZrO_2 supported Cu.

There were no detectable Cu XRD diffraction peaks (**Figure S2** in Supporting Information), suggesting a well dispersed metal phase [45]. This is consistent with microscopy analysis; STEM micrographs are presented in **Figure 4(I)** with associated Cu histograms **(II)** for Cu/SiO_2 **(a)** and Cu/TiO_2 **(b)**, as representative samples. Both catalysts exhibit Cu particles ≤5 nm with a similar mean size (2-3 nm). The characterisation measurements suggest similar properties for the supported Cu phase in all the catalysts.

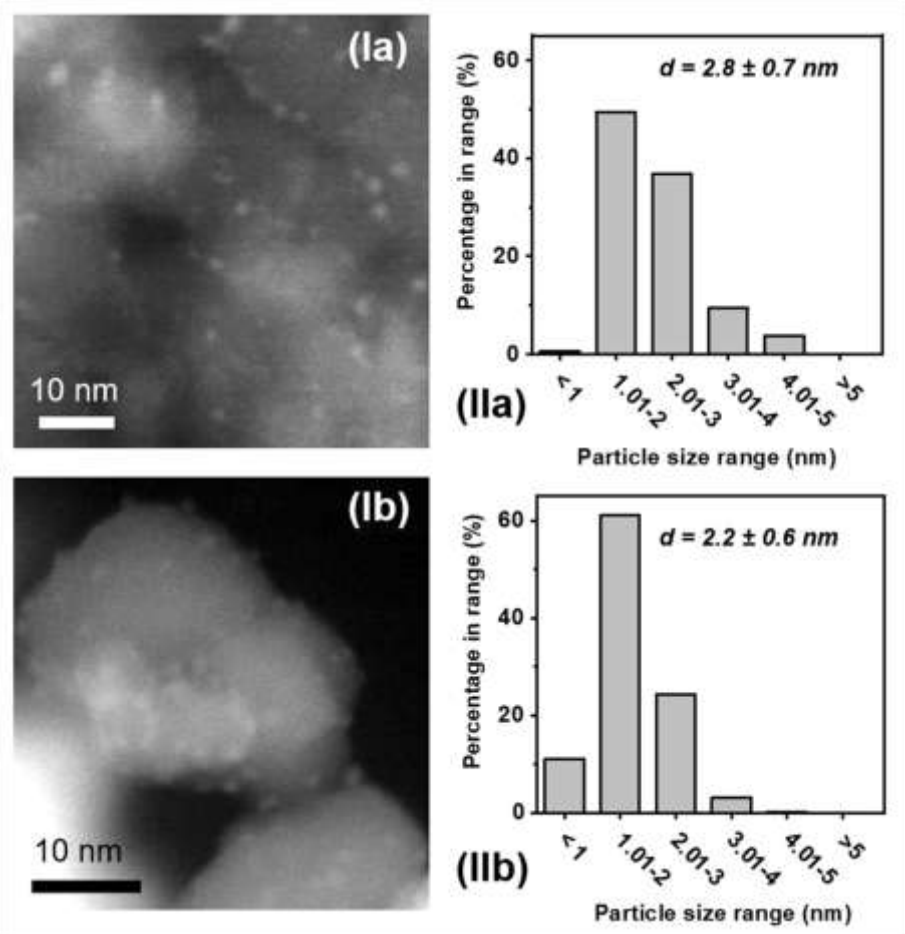

Figure 4: **(I)** Representative STEM and **(II)** associated Cu particle size distributions for **(a)** Cu/SiO_2 and **(b)** Cu/TiO_2.

All the Cu catalysts exhibited an essentially time-invariant activity (see results for Cu/Al_2O_3 and Cu/TiO_2, as representatives, in the inset to **Figure 5**) and 100% selectivity to the target 2-butanone with no evidence of dehydration ((path **II**) in **Figure1(b)**) or dimerisation (path **III**)). The combined ultra-selectivity and catalyst stability achieved in this work represents a net improvement compared with reported selectivity to 2-butanone (50-90%) over Cu catalysts in both liquid- [64] and gas-phase operation [65] and deactivation with time on-stream over Ni colloids [66]. The dehydrogenation of aliphatic alcohols over supported Cu is structure sensitive [67] and proceeds *via* a two-step mechanism [48] involving heterolytic cleavage of the O-H bond [68] and abstraction of the second H in α-position [22]. Alcohol

adsorption/activation occurs at the Cu-oxide interface with the α-hydrogen interacting with Cu and the hydrogen-end of the hydroxyl group binding to support Lewis basic (oxygen anion) sites [22]. The removal of the first H with the formation of a surface alkoxide [69] is rate determining [70] and should be sensitive to oxide Lewis basicity. This, in turn, is related to the partial negative charge of the oxygen in the oxide ($-q_O$) which can be calculated [71,72] (see Supporting Information) and a higher $-q_O$ reflects greater Lewis basicity [73].

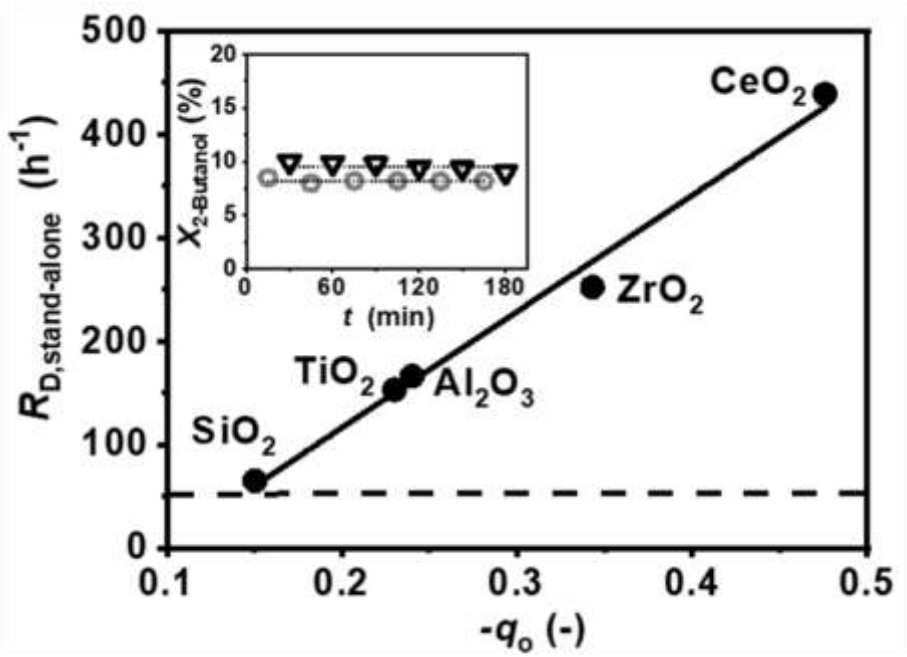

Figure 5: Dependence of hydrogen production rate ($R_{D,stand\text{-}alone}$; h^{-1}; ●) from 2-butanol dehydrogenation on the partial negative charge of oxygen in the oxide support ($-q_o$). *Inset*: Variation of 2-butanol conversion ($X_{2\text{-}Butanol}$) with time on-stream (t) over Cu/Al_2O_3 (▽) and Cu/TiO_2 (○), as representative samples. *Note:* Horizontal dashed line represents specific hydrogen consumption rate in stand-alone furfural hydrogenation ($R_{H,stand\text{-}alone}$) over Au/CeO_2 using an external H_2 supply. Solid and dotted lines (inset) provide a guide to aid visual assessment; *Reaction conditions: T = 453 K, P = 1 atm.*

We quantify dehydrogenation activity in terms of hydrogen production rate and the dependence on $-q_O$ is presented in **Figure 5**. Hydrogen produced was 2-10 times greater than that consumed in furfural hydrogenation over Au/CeO_2 (dashed line in **Figure 5**) under the same reaction conditions. We observe a linear increase of

activity with increasing $-q_O$ (from Cu/SiO_2 = 0.15 to Cu/CeO_2 = 0.48). A greater Lewis basicity of the oxide oxygen anion (*i.e.* higher $-q_O$) facilitates hydrogen extraction from the hydroxyl group in 2-butanol to form the alkoxide intermediate which, in turn, increases dehydrogenation rate. In support of this, there is evidence in the literature of greater (oxidative) dehydrogenation rates in the conversion of substituted benzyl alcohol with electron donating groups (*vs.* aliphatic alcohols) linked to a more facile removal of the acidic hydroxyl H on surface basic sites of a hydrotalcite catalyst [74].

We first examined the coupled dehydrogenation-hydrogenation (2-butanol + furfural in N_2) over Au/CeO_2 and Cu-based catalysts in separate runs. There was no coupling to produce furfuryl alcohol over Au/CeO_2 and limited hydrogenation activity ($R_{H,coupling} \leq 14$ h^{-1}) over all supported Cu catalysts. This demonstrates that only Au or Cu cannot promote both steps (dehydrogenation and hydrogenation) in the coupled reaction.

3.3 Coupled 2-Butanol-furfural Dehydrogenation-hydrogenation

The concentration and mobility of reactive surface hydrogen supply to Au determines furfural consumption rate in the coupled process. Hydrogen generated *in* situ (*via* 2-butanol dehydrogenation over Cu) can diffuse across a solid-solid boundary [75,76] or desorb associatively and travel in between multiple catalyst beds in series to participate in hydrogenation reactions [77,78]. We examined the coupled process in these two configurations using (i) a two catalytic bed arrangement with Cu/CeO_2 (highest dehydrogenation rate among the Cu catalysts) on top and Au/CeO_2 (active in furfural hydrogenation) below (Cu:Au molar ratio = 12; see details in **Experimental** section) and (ii) a physical mixture of Cu/CeO_2+Au/CeO_2 in a single bed. Adopting the 2-bed arrangement, we observe the formation of furfuryl alcohol and 2-butanone as the only detected products. This result proves that hydrogen

generated over Cu/CeO_2 is transferred and borrowed by gold. In line with this, hydrogen desorption *at* $T < 453$ K was proven using temperature programmed desorption (H_2-TPD) by Liu *et al.* (over Ru/CeO_2) [79] and Sepúlveda-Escribano *et al.* (Pt/CeO_2) [80]. In terms of activity, we recorded a similar conversion with time on-stream profile (see **Figure S1** in Supporting Information) and hydrogenation rate relative to that in the stand-alone hydrogenation of furfural over Au/CeO_2. This result indicates that hydrogenation activity is governed by the Au component where the hydrogen dissociation/activation capacity of gold determines surface hydrogen concentration and hydrogenation rate. Coupled reaction over Cu/CeO_2 and Au/CeO_2 in two separate beds was accompanied by a greater H_2 utilisation efficiency (from 432 to 3) and a (2-fold) lower E-factor (=215) relative to stand-alone hydrogenation over Au/CeO_2. Full selectivity to target 2-butanone/furfuryl alcohol was retained in the coupled dehydrogenation/hydrogenation of 2-butanol/furfural over a (single bed) Cu/CeO_2+Au/CeO_2 physical mixture (Cu:Au molar ratio = 12). We recorded a significant (28-fold) increase in specific (per mol of Au) hydrogenation activity which demonstrates the formation of activated H species in the dehydrogenation step [81] over Cu/CeO_2 that travel across the CeO_2 support [82] and participate in the hydrogenation of furfural over Au/CeO_2. This served to overcome the "inefficient" H_2 activation step by Au (required in the stand-alone process and with a 2-bed configuration), resulting in higher hydrogenation rate, with full hydrogen utilization and a lower associated E-factor (=15).

Hydrogen generation is critical but hydrogenation response is also dependant on hydrogen transfer (between Cu → Au and across the CeO_2) which can be influenced by interactions with the support [25]. In order to evaluate the possible support effects in coupled dehydrogenation/hydrogenation process we have assessed the catalytic

action of physical mixtures containing Au/CeO_2 with added Cu/oxide catalysts in a single bed configuration; the results are shown in **Figure 6**. Full selectivity to furfuryl alcohol and 2-butanone and a (2-28 fold) greater hydrogenation rate (relative to the stand-alone hydrogenation over Au/CeO_2) was attained over each physical mixture. The linear correlation between hydrogen supplied (from 2-butanol dehydrogenation) and hydrogenation rate (**Figure 6(I)**) proves that furfural hydrogenation in the coupling process is controlled by hydrogen generation in the dehydrogenation step. Yang *et al.* [83] linked the observed increase of nitro group hydrogenation rate in the coupling process (ammonia borane dehydrogenation with substituted nitrobenzenes hydrogenation) *vs.* stand-alone hydrogenation to the high hydrogen generation rate *via* ammonia borane dehydrogenation.

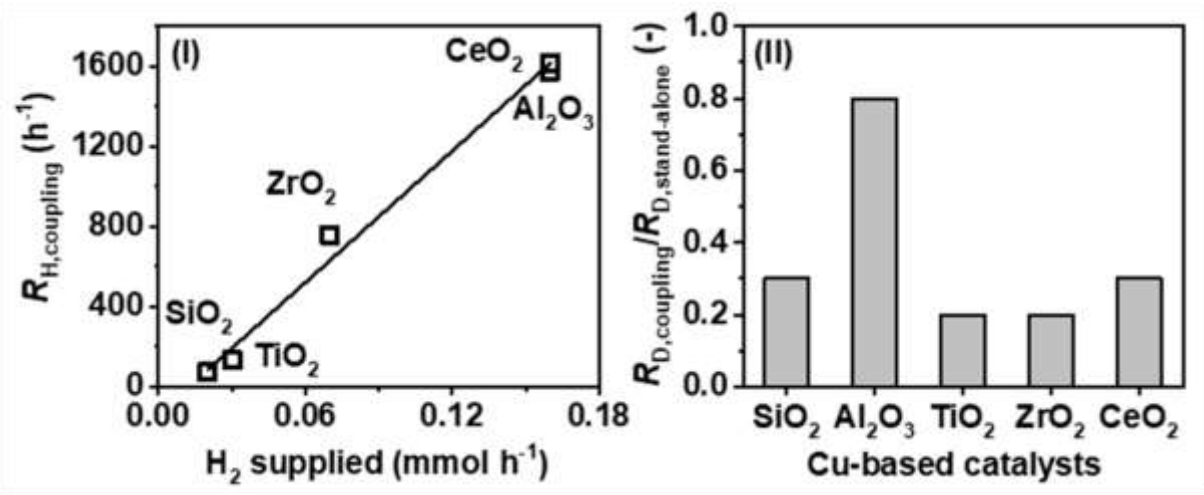

Figure 6: (I) Dependence of furfural hydrogenation rate ($R_{\mathbf{H,\ coupling}}$; h^{-1}; □) on the amount of hydrogen supplied (mmol h^{-1}) from 2-butanol dehydrogenation in the coupled process over physical mixtures of Cu/oxide+Au/CeO_2 and **(II)** variation in 2-butanol dehydrogenation rate in the coupling process ($R_{\mathbf{D,coupling}}$) relative to that in stand-alone reaction ($R_{\mathbf{D,stand\text{-}alone}}$) for reaction over Cu/oxide+Au/CeO_2 and Cu/oxide, respectively. *Reaction conditions: T* = 453 K, *P* = 1 atm, Cu:Au = 12

We compared the specific (per mol of Cu) dehydrogenation activity in the coupling process over Cu+Au physical mixtures ($R_{D,coupling}$) with that in the stand-alone dehydrogenation of 2-butanol ($R_{D,stand\text{-}alone}$) over the oxide supported Cu

catalysts and the results obtained are shown in **Figure 6(II)**. The greater hydrogen production in the stand-alone dehydrogenation over all the catalysts is indicative of competition between furfural and 2-butanol for adsorption sites [84] that must result in a displacement of 2-butanol by furfural. This is consistent with experimental work that has demonstrated a higher adsorption strength for furfural compared to alcohols on the surface of Cu/SiO_2 [85]. Panagiotopoulou *et al.* [86] concluded a similar inhibiting effect of furfural using a series of alcohols (2-propanol, 2-butanol and 2-pentanol) in the liquid phase production of 2-methylfuran. It should be noted that Cu/Al_2O_3 deviates somehow from the general trend with an almost equivalent dehydrogenation activity in the coupling process and stand-alone reaction. We tentatively attribute this response to the presence of low-coordination oxygen atoms on the surface of Al_2O_3 [87,88] that can act as additional adsorption/activation sites for the -C=O functionality in furfural *via* nucleophilic attack at the polarised $C^{\delta+}$ [84].

Taking the five physical mixtures presented in **Figure 6**, H_2 utilisation efficiency decreased in the order: Au/CeO_2+Cu/CeO_2 (1.00) > Au/CeO_2+Cu/ZrO_2 (1.02) > Au/CeO_2+Cu/Al_2O_3 (1.19) > Au/CeO_2+Cu/TiO_2 (2.40) > Au/CeO_2+Cu/SiO_2 (3.34). These results indicate that the reducibility of the carrier does not impact significantly on hydrogen utilisation efficiency. Indeed, a similar hydrogen utilisation was obtained over (reducible) CeO_2 and (non-reducible) Al_2O_3 supported Cu systems. Taking (non-reducible) Al_2O_3 and SiO_2 we obtained a significant (36%) difference in hydrogen usage. It is well-known [89] that carbonaceous materials (*e.g.* carbon layers or coke) can facilitate hydrogen spillover across oxides by transfer as a proton-electron couple (*i.e.* enhanced mobility compared with transfer as H atoms) [26]. All the supported Cu catalysts exhibited an initial decline in activity with time on-stream to attain a pseudo-steady state after *ca.* 90 min (**Figure 7(I)**). The degree of

catalyst deactivation in the coupling process was quantified in terms of % of activity lost between initial and steady state conversion. Cu/CeO_2 and Cu/Al_2O_3 exhibited the highest deactivation (~8%) while Cu/SiO_2 and Cu/TiO_2 showed a similar (high) stability (~1% deactivation). The observed temporal decrease in dehydrogenation activity can be attributed to coke formation, notably on acid sites of the carrier [90], during furfural conversion [91] over (*e.g.* SiO_2 [92] and Al_2O_3 [93]) supported Cu catalysts. The possible formation of carbonaceous deposits was evaluated by thermogravimetric analysis (TGA) analysis; the results for Cu/SiO_2 **(a)** and Cu/Al_2O_3 **(b)**, as representatives, are shown in **Figure 7(II)**.

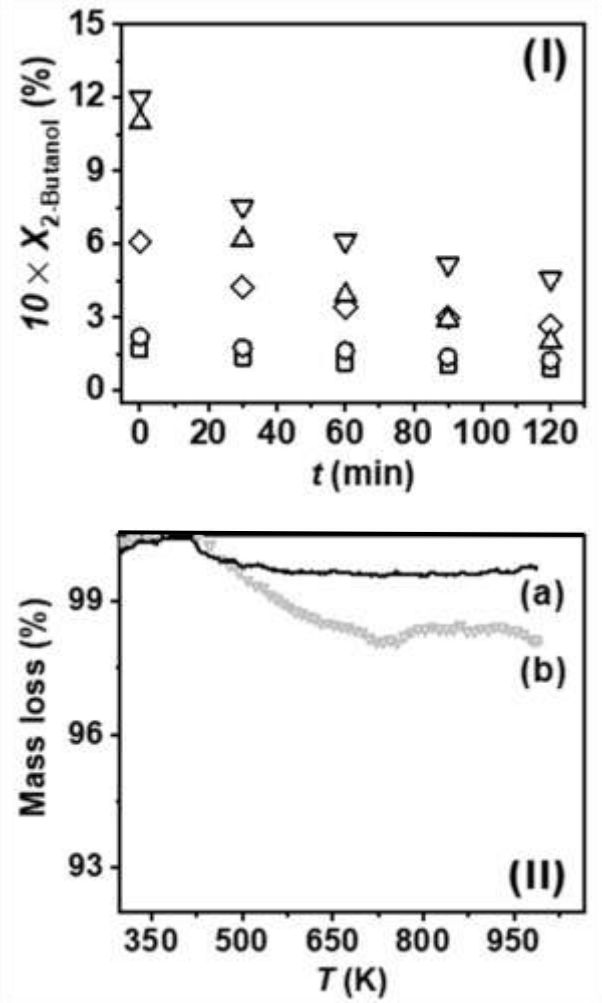

Figure 7: (I) Variation of 2-butanol conversion ($X_{2\text{-Butanol}}$) with time on-stream (t, min) in the coupling process over physical mixtures of Au/CeO_2 with Cu/Al_2O_3 (▽), Cu/CeO_2 (△), Cu/ZrO_2 (◇), Cu/TiO_2 (●) and Cu/SiO_2 (■). **(II)** Thermogravimetric

analysis (TGA) profiles generated during thermal treatment (in N_2) of spent **(a)** Cu/SiO_2 (solid line) and **(b)** Cu/Al_2O_3 (▽). *Reaction conditions: T* = 453 K*, P* = 1 atm.

The fresh (activated in H_2) catalyst was carried through as a reference and the signals corrected to ensure that the profiles shown refer solely to carbon deposition during the coupled process. Both spent catalysts displayed a high temperature (>420-700 K) mass loss that can be linked to decomposition of "soft coke" (see **Experimental** section) generated during furfural conversion [29,30]. Over the same temperature range, we observe a (3-fold) greater mass loss over Cu/Al_2O_3 relative to Cu/SiO_2 that can be linked to increased coke accumulation on the more acidic alumina. Likewise, Wan and co-workers [94] studying the synthesis of gasoline from methanol showed (by TGA analysis) higher (3.1% *vs.* 0.5%) coke concentration over zeolites with low (23 *vs.* 217) SiO_2/Al_2O_3 ratio attributed to differences in acidity. The presence of carbonaceous deposits on the surface of Al_2O_3 facilitates hydrogen transfer in a similar manner to that on reducible supports as a proton-electron couple which, in turn, results in enhanced hydrogenation utilization efficiency.

Au/CeO_2+Cu/CeO_2, which delivered the best combined hydrogenation rate and hydrogen utilisation efficiency, was employed for further analyses. Catalytic coupling over a physical mixture of Cu/CeO_2+Au/CeO_2, varying the Cu/Au ratio, gave the results presented in **Figure 8.** In each case, 100% of selectivity to the target 2-butanone and furfuryl alcohol products was achieved.

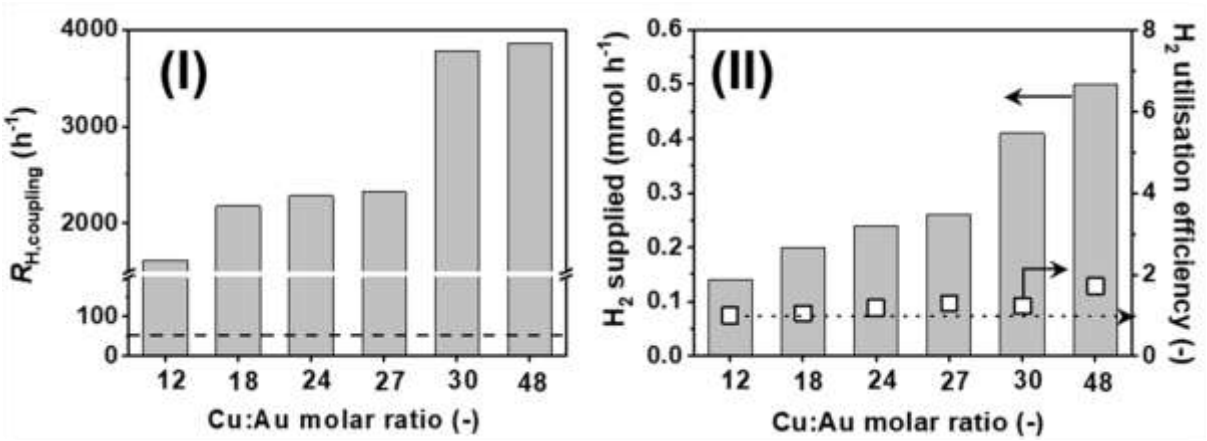

Figure 8: Catalytic results for coupled reaction over a Cu/CeO_2+Au/CeO_2 physical mixture in terms of **(I)** rate of furfuryl alcohol production ($R_{H,coupling}$; h^{-1}) and **(II)** quantity of hydrogen supplied (mmol h^{-1}) *via* 2-butanol dehydrogenation and H_2 utilisation efficiency (□, see Eqn. **5**) as a function of Cu:Au molar ratio. *Note*: horizontal dashed line in **(I)** represents specific hydrogen consumption rate in stand-alone furfural hydrogenation over Au/CeO_2 using an external H_2 supply; dashed arrow in **(II)** indicates full H_2 utilisation efficiency under stoichiometric conditions. *Reaction conditions*: T = 453 K, P = 1 atm

The rate of furfuryl alcohol production was enhanced (from 1600 h^{-1} to 3800 h^{-1}) with increasing Cu:Au (from 12 to 30) (**(I)**). This is an important result as it represents a 70-fold greater hydrogenation rate relative to reaction over Au/CeO_2 using an external H_2 supply (dashed line in **(I)**). The dependence of hydrogenation rate on Cu:Au ratio coincided with that observed for hydrogen generation from 2-butanol dehydrogenation (**Figure 6(I)**). Hydrogen utilisation efficiency converged at reaction stoichiometry, *i.e.* full usage by Au/CeO_2 of the hydrogen generated by Cu/CeO_2 (dotted arrow in **(II)**). Reaction at higher Cu:Au (=48) served to increase hydrogen generation with only a marginal increase in furfuryl alcohol production rate. Full H_2 utilisation was not achieved in this case, which can be attributed to insufficient Au to promote the hydrogenation step. The coupled process significantly lowered (215-fold) the E-factor to 2, which is at the lower end of the range (5->50) in the fine chemical sector [27].

4. Conclusions

Au/CeO_2 (mean Au size = 3.5 nm) promotes the continuous gas phase hydrogenation of furfural exclusively to furfuryl alcohol but less than 1% of the hydrogen supplied is utilised in the reaction. A series of oxide (Al_2O_3, ZrO_2, SiO_2, TiO_2 and CeO_2) supported Cu (2-4% wt.) catalysts were prepared by deposition-precipitation to deliver *post*-H_2-TPR metal nanoparticles with a mean size of 2-3 nm (from STEM). All the Cu catalysts promoted the sole formation of 2-butanone in the dehydrogenation of 2-butanol. The partial negative charge of the oxygen in the support correlated with hydrogen production rate where Cu/CeO_2 delivered the highest dehydrogenation activity. A series of Au/CeO_2+Cu/Oxide physical mixtures promoted exclusive formation of 2-butanone and furfuryl alcohol in coupled dehydrogenation-hydrogenation (of 2-butanol/furfural), where surface coverage by carbonaceous deposits facilitates hydrogen transfer, enhancing hydrogen utilisation efficiency. The combination Au/CeO_2+Cu/CeO_2 delivered full hydrogen utilisation and a 70-fold greater furfuryl alcohol production rate relative to conventional hydrogenation over Au/CeO_2. Higher sustainability of the coupling process (*vs.* standard hydrogenation) is demonstrated with a significantly lower E-factor = 2 (*vs.* 430). Our results establish the basis for the development of a continuous alternative route for the sustainable production of high value chemicals *via* single-pot coupled dehydrogenation-hydrogenation.

Acknowledgements

We would like to thank the Engineering and Physical Sciences Research Council, University of Heriot-Watt, and CRITICAT Centre for Doctoral Training for financial support [Ph.D. studentship to Chiara Pischetola; Grant EP/L016419/1].

References

[1] W. Bonrath, CHIMIA Int. J. Chem. 68 (2014) 485-491.

[2] F. Schüth, in: R. Rinaldi (Ed.), Catalytic Hydrogenation for Biomass Valorization, Royal Society of Chemistry, Cambridge, 2014, p. 310.

[3] D. Wang, D. Astruc, Chem. Rev. 115 (2015) 6621-6686.

[4] J. Muzart, Eur. J. Org. Chem. 2015 (2015) 5693-5707.

[5] K. Yamaguchi, J. L. He, T. Oishi, N. Mizuno, Chem. A Eur. J. 16 (2010) 7199-7207.

[6] J. Li, J. L. Liu, H. J. Zhou, Y. Fu, ChemSusChem 9 (2016) 1339-1347.

[7] Y. Huang, W. M. H. Sachtler, J. Catal. 190 (2000) 69-74.

[8] W. Gong, C. Chen, R. Fan, H. Zhang, G. Wang, H. Zhao, Fuel 231 (2018) 165-171.

[9] M. J. Gilkey, B. Xu, ACS Catal. 6 (2016) 1420-1436.

[10] I. Gandarias, P. L. Arias, S. G. Fernández, J. Requies, M. El Doukkali, M. B. Güemez, Catal. Today 195 (2012) 22-31.

[11] M. Chia, J. A. Dumesic, Chem. Commun. 47 (2011) 12233-12235.

[12] H. Chen, H. Ruan, X. Lu, J. Fu, T. Langrish, X. Lu, Mol. Catal. 445 (2018) 94-101.

[13] S. M. A. H. Siddiki, T. Toyao, K. I. Shimizu, Green Chem. 20 (2018) 2933-2952.

[14] G. Machado, S. Leon, F. Santos, R. Lourega, J. Dullius, M. E. Mollmann, P. Eichler, Nat. Resour. 7 (2016) 115-129.

[15] M. G. Bramucci, D. Flint, E. S. Miller, V. Nagarajan, N. Sedkova, M. Singh, T. K. Van Dyk, Method for the Production of 2-Butanol (2008) US 2008/0274525 A1

[16] A. Astashkina, Y. Kolbysheva, A. Nikiforova, A. Bakibayev, MATEC Web Conf. 85 (2016) 0102201-0102209.

[17] R. V. Sharma, U. Das, R. Sammynaiken, A. K. Dalai, Appl. Catal. A: Gen. 454 (2013) 127-136.

[18] C. L. Yaws, The Yaws Handbook of Physical Properties for Hydrocarbons and Chemicals: Physical Properties for More than 54,000 Organic and Inorganic Chemical Compounds, Coverage for C1 to C100 Organics and Ac to Zr Inorganics, Elsevier, Oxford, 2015.

[19] M. Li, L. Collado, F. Cárdenas-Lizana, M. A. Keane, Catal. Lett. 148 (2017) 90-96.

[20] J. R. Ruiz, C. Jiménez-Sanchidrián, Curr. Org. Chem. 11 (2007) 1113-1125.

[21] M. A. Keane, M. Li, L. Collado, F. Cárdenas-Lizana, Reac. Kinet. Mech. Cat. 125 (2018) 25-36.

[22] R. Shi, F. Wang, Tana, Y. Li, X. Huang, W. Shen, Green Chem. 12 (2010) 108-113.

[23] S. A. Halawy, M. A. Mohamed, S. F. A. El-Hafez, J. Mol. Catal. 94 (1994) 191-201.

[24] W. Fang, J. Chen, Q. Zhang, W. Deng, Y. Wang, Chem. Eur. J. 17 (2011) 1247-1256.

[25] C. Y. Wang, C. W. Chang, Y. J. Wu, A. D. Lueking, Curr. Opin. Chem. Eng. 21 (2018) 116-121.

[26] W. Karim, C. Spreafico, A. Kleibert, J. Gobrecht, J. VandeVondele, Y. Ekinci, J. A. van Bokhoven, Nature 541 (2017) 68-71.

[27] R. A. Sheldon, ACS Sust. Chem. Eng. 6 (2018) 32-48.

[28] E. Nino, A. Lapena, J. Martinez, J. M. Gutierrez, S. Mendioroz, J. L. G. Fierro, J. A. Pajares, in: G. Poncelet, P. Grange, P.A. Jacobs (Eds.), Studies in Surface Science and Catalysis, Elsevier, 1983, p. 747.

[29] Y. Li, C. Zhang, Y. Liu, X. Hou, R. Zhang, X. Tang, Energy Fuels 29 (2015) 1722-1728.

[30] H. Zhang, S. Shao, R. Xiao, D. Shen, J. Zeng, Energy Fuels 28 (2014) 52-57.

[31] A. R. Pradhan, J. F. Wu, S. J. Jong, T. C. Tsai, S. B. Liu, Appl. Catal. A: Gen. 165 (1997) 489-497.

[32] M. Li, Y. Hao, F. Cárdenas-Lizana, M. A. Keane, Catal. Commun. 69 (2015) 119-122.

[33] A. González-Fernández, C. Pischetola, L. Kiwi-Minsker, F. Cárdenas-Lizana, J. Phys. Chem. C 124 (2020) 3681-3691.

[34] I. Hachemi, K. Jeništova, P. Mäki-Arvela, N. Kumar, K. Eranen, J. Hemming, D. Y. Murzin, Catal. Sci. Technol. 6 (2016) 1476-1487.

[35] S. Y. Lai, Y. Qiu, S. Wang, J. Catal. 237 (2006) 303-313.

[36] M. Ousmane, L. F. Liotta, D. di Carlo, G. Pantaleo, A. M. Venezia, G. Deganello, L. Retailleau, A. Boreave, A. Giroir-Fendler, Appl. Catal. B: Environ. 101 (2011) 629-637.

[37] J. Ohyama, A. Esaki, Y. Yamamoto, S. Arai, A. Satsuma, RSC Adv. 3 (2013) 1033-1036.
[38] R. van Hardeveld, F. Hartog, Surf. Sci. 15 (1969) 189-230.
[39] C. Kartusch, J. A. van Bokhoven, Gold Bull. 42 (2009) 343-348.
[40] K. Yan, G. Wu, T. Lafleur, C. Jarvis, Renew. Sust. Energ. Rev. 38 (2014) 663-676.
[41] V. V. Pushkarev, N. Musselwhite, K. An, S. Alayoglu, G. A. Somorjai, Nano Lett. 12 (2012) 5196-5201.
[42] Y. Nakagawa, H. Nakazawa, H. Watanabe, K. Tomishige, ChemCatChem 4 (2012) 1791-1797.
[43] P. Anastas, N. Eghbali, Chem. Soc. Rev. 39 (2010) 301-312.
[44] R. Zanella, C. Louis, S. Giorgio, R. Touroude, J. Catal. 223 (2004) 328-339.
[45] G. C. Bond, Gold Bull. 49 (2016) 53-61.
[46] S. Gómez-Quero, F. Cárdenas-Lizana, M. A. Keane, Ind. Eng. Chem. Res. 47 (2008) 6841-6853.
[47] E. Bus, J. T. Miller, J. A. van Bokhoven, J. Phys. Chem. B 109 (2005) 14581-14587.
[48] V. Z. Fridman, A. A. Davydov, K. Titievsky, J. Catal. 222 (2004) 545-557.
[49] K. Shimizu, N. Imaiida, K. Kon, S. Siddiki, A. Satsuma, ACS Catal. 3 (2013) 998-1005.
[50] K. Kon, S. M. A. H. Siddiki, K. I. Shimizu, J. Catal. 304 (2013) 63-71.
[51] W. C. Conner, J. L. Falconer, Chem. Rev. 95 (1995) 759-788.
[52] F. Röbner, in: H.K. G. Ertl, F. Schütz, J. Weitkamp (Ed.), Handbook of Heterogeneous Catalysis, Wiley-VCH, Weinheim, 2008, p. 1051.
[53] C. V. Pramod, C. Raghavendra, K. H. P. Reddy, G. V. R. Babu, K. S. R. Rao, B. D. Raju, J. Chem. Sci. 126 (2014) 311-317.
[54] N. P. Tangale, P. S. Niphadkar, S. S. Deshpande, P. N. Joshi, Appl. Catal. A: Gen. 467 (2013) 421-429.
[55] V. Z. Fridman, A. A. Davydov, J. Catal. 195 (2000) 20-30.
[56] C. Liu, Y. Wang, H. Chu, M. Qiu, L. Niu, G. Bai, Chin. J. Chem. 32 (2014) 1281-1286.
[57] M. V. Morales, E. Asedegbega-Nieto, B. Bachiller-Baeza, A. Guerrero-Ruiz, Carbon 102 (2016) 426-436.
[58] G. Águila, F. Gracia, P. Araya, Appl. Catal. A: Gen. 343 (2008) 16-24.

[59] K. K. Bando, K. Sayama, H. Kusama, K. Okabe, H. Arakawa, Appl. Catal. A: Gen. 165 (1997) 391-409.

[60] S. S. Hong, G. H. Lee, G. D. Lee, Korean J. Chem. Eng. 20 (2003) 440-444.

[61] Y. Hu, L. Dong, M. Shen, D. Liu, J. Wang, W. Ding, Y. Chen, Appl. Catal. B: Environ. 31 (2001) 61-69.

[62] S. Y. Liu, S. M. Yang, Appl. Catal. A: Gen. 334 (2008) 92-99.

[63] T. K. Nevanperä, S. Ojala, N. Bion, F. Epron, R. L. Keiski., Appl. Catal. B: Environ. 182 (2016) 611-625.

[64] Z. Wang, H. Ma, W. Zhu, G. Wang, React. Kinet. Catal. Lett. 76 (2002) 271-279.

[65] E. Geravand, Z. Shariatinia, F. Yaripour, S. Sahebdelfar, Korean J. Chem. Eng. 32 (2015) 2418-2428.

[66] J. Gao, F. Guan, Y. Zhao, W. Yang, Y. Ma, X. Lu, J. Hou, J. Kang, Mat. Chem. Phys. 71 (2001) 215-219.

[67] S. Lambert, C. Cellier, F. Ferauche, E. M. Gaigneaux, B. Heinrichs, Catal. Commun. 8 (2007) 2032-2036.

[68] M. M. Branda, A. H. Rodríguez, P. G. Belelli, N. J. Castellani, Surf. Sci. 603 (2009) 1093-1098.

[69] M. L. Bailly, C. Chizallet, G. Costentin, J. M. Krafft, H. Lauron-Pernot, M. Che, J. Catal. 235 (2005) 413-422.

[70] R. M. Rioux, M. A. Vannice, J. Catal. 216 (2003) 362-376.

[71] A. C. C. Rodrigues, J. Math. Chem. 37 (2005) 347-351.

[72] N. C. Jeong, J. S. Lee, E. L. Tae, Y. J. Lee, K. B. Yoon, Angew. Chem. 120 (2008) 10282-10286.

[73] H. Idriss, M. A. Barteau, in: B.C. Gates, H. Knözinger (Eds.), Advances in Catalysis. Impact or Surface Science on Catalysis, Academic Press, 2000, p. 261.

[74] W. Zhou, Q. Tao, J. Pan, J. Liu, J. Qian, M. He, Q. Chen, J. Mol. Catal. A: Chem. 425 (2016) 255-265.

[75] R. B. Levy, M. Boudart, J. Catal. 32 (1974) 304-314.

[76] D. Nabaho, J. W. Niemantsverdriet, M. Claeys, E. van Steen, Catal. Today 261 (2016) 17-27.

[77] G. García-Colli, J. A. Alves, O. M. Martínez, G. F. Barreto, Chem. Eng. Process. 105 (2016) 38-45.

[78] Y. Hao, M. Li, F. Cárdenas-Lizana, M. A. Keane, Catal. Lett. 146 (2016) 109-116.

[79] P. Liu, R. Niu, W. Li, S. Wang, J. Li, Energ. Source. Part A 41 (2019) 689-699.

[80] A. A. Sepúlveda-Escribano, J. Silvestre-Albero, F. Coloma, F. Rodríguez-Reinoso, in: A. Corma, F.V. Melo, S. Mendioroz, J.L.G. Fierro (Eds.), Studies in Surface Science and Catalysis, Elsevier, 2000, p. 1013.

[81] M. E. Crivello, C. F. Pérez, S. N. Mendieta, S. G. Casuscelli, G. A. Eimer, V. R. Elías, E. R. Herrero, Catal. Today 133 (2008) 787-792.

[82] Y. Nakagawa, S. Tazawa, T. Wang, M. Tamura, N. Hiyoshi, K. Okumura, K. Tomishige, ACS Catal. 8 (2018) 584-595.

[83] Q. Yang, Y. Z. Chen, Z. U. Wang, Q. Xu, H. L. Jiang, Chem. Commun. 51 (2015) 10419-10422.

[84] A. Saadi, Z. Rassoul, M. M. Bettahar, J. Mol. Catal. A: Chem. 164 (2000) 205-216.

[85] S. Sitthisa, T. Sooknoi, Y. Ma, P. B. Balbuena, D. E. Resasco, J. Catal. 277 (2011) 1-13.

[86] P. Panagiotopoulou, N. Martin, D. G. Vlachos, J. Mol. Catal. A: Chem. 392 (2014) 223-228.

[87] E. F. Archibong, A. St-Amant, J. Phys. Chem. A 103 (1999) 1109-1114.

[88] I. Manassidis, A. De Vita, M. J. Gillan, Surf. Sci. Lett. 285 (1993) L517-L521.

[89] R. Prins, V. K. Palfi, M. Reiher, J. Phys. Chem. C 116 (2012) 14274-14283.

[90] S. Srihiranpullop, P. Praserthdam, Catal. Today 93-95 (2004) 723-727.

[91] Z. Xinghua, W. Tiejun, M. Longlong, W. Chuangzhi, Fuel 89 (2010) 2697-2702.

[92] D. Vargas-Hernández, J. M. Rubio-Caballero, J. Santamaría-González, R. Moreno-Tost, J. M. Mérida-Robles, M. A. Pérez-Cruz, A. Jiménez-López, R. Hernández-Huesca, P. Maireles-Torres, J. Mol. Catal. A: Chem. 383-384 (2014) 106-113.

[93] S. Park, H. P. R. Kannapu, C. Jeong, J. Kim, Y.-W. Suh, ChemCatChem 12 (2020) 111-105.

[94] Z. Wan, W. Wu, G. Li, C. Wang, H. Yang, D. Zhang, Appl. Catal. A: Gen. 523 (2016) 312-320.